Electro-optical measurements of picosecond bunch length of a 45 MeV electron beam

T. Tsang[a], V. Castillo, R. Larsen, D. M. Lazarus, D. Nikas, C. Ozben, Y. K. Semertzidis, and T. Srinivasan-Rao
Brookhaven National Laboratory, Upton, New York 11973

L. Kowalski
Montclair State University, Upper Montclair, New Jersey 07043

(Received 4 October 2000; accepted for publication 29 January 2001)

We have measured the temporal duration of 45 MeV picosecond electron beam bunches using a noninvasive electro-optical (EO) technique. The amplitude of the EO modulation was found to increase linearly with electron beam charge and decrease inversely with distance from the electron beam. The rise time of the temporal signal was limited by our detection system to ~70 ps. The EO signal due to ionization caused by the electrons traversing the EO crystal was also observed. It has a distinctively long decay time constant and signal polarity opposite to that due to the field induced by the electron beam. The electro-optical technique may be ideal for the measurement of bunch length of femtosecond, relativistic, high energy, charged, particle beams. © *2001 American Institute of Physics.* [DOI: 10.1063/1.1358322]

I. INTRODUCTION

With the advance of electron and particle accelerators, the particle bunch duration has dropped to the femtosecond time scale. Various techniques have been proposed to measure such ultrashort bunch lengths. One of the techniques relies on noncoherent transition radiation where visible photons are collected and measured with a streak camera.[1] Although such a technique can yield bunch length information, it is an invasive technique and the resolution is sensitive to the photon collection system. Recently, the development of the electro-optical (EO) probe based on the linear Pockels effect has revolutionized the noninvasive measurements of small electronic signal propagation on integrated circuits,[2,3] dc and ac high voltages,[4–6] lightning detectors,[7] terahertz electromagnetic field imaging,[8]and electron beam measurements of long pulse[9] and short pulse duration.[10–14] EO sensors that use fibers for input and output coupling provide excellent electromagnetic isolation and large frequency response, limited essentially by the fibers and the velocity mismatch of the electrical and optical waves to picosecond or subpicosecond time resolution. In this work we show that the fast component of the EO modulation is due only to the transient electric field induced by the passage of an ultrashort relativistic electron bunch. No cavity mode[14] was observed. We examine the dependence of the EO modulation with charge and its position. Finally, we present a detection-limited temporal shape of the EO signal and then draw our conclusions regarding the electron bunch length.

The optical probe is based on the principle of the linear electro-optical effect, Pockels effect. When an electric field is applied to a birefringent crystal, the refractive index ellipsoid is modulated and an optical phase shift is introduced. To probe the phase shift, an optical beam polarized at 45° to the z axis of the EO crystal is propagated along the y axis of the crystal. This phase retardation is converted to an intensity modulation by a $\lambda/4$ wave plate followed by an analyzer (crossed polarizer). The intensity of light $I(t)$ transmitted through the analyzer can be described by[15]

$$I(t)=I_o[\,\eta+\sin^2(\Gamma_o+\Gamma_b+\Gamma(t))], \tag{1}$$

where I_o is the input light intensity, η contains the scattering contribution of the EO crystal and the imperfection of the polarizer and other optics which are typically much less than 1, Γ_o contains the residual birefringence of the crystal, Γ_b is the optical bias of the system which is set at $\pi/4$, and $\Gamma(t)$ is the optical phase induced by the electric field imparted on the crystal. When $\Gamma_o+\Gamma_b\simeq\pi/4$, Eq. (1) can be written as

$$\frac{I(t)}{I_o}\simeq\left(\eta+\frac{1}{2}\right)+\left[\frac{1}{2}\sin(2\Gamma(t))\right], \tag{2}$$

where the first term is the unmodulated dc light level which is approximately equal to half of the input light intensity, and the second term is the EO modulation. For a weak modulation, i.e., $2\Gamma(t)\ll 1$, the EO component can be written as

$$\left[\frac{I(t)}{I_o}\right]_{\mathrm{EO}}\simeq\Gamma(t). \tag{3}$$

The normalized light output is approximately linear in the time-dependent optical phase.

The transient optical phase shift is linearly proportional to the time-dependent field $E_z(t)$ traversing the optical axis of the EO crystal and can be expressed as

[a]Electronic mail: Tsang@bnl.gov

$$\Gamma(t)=\frac{1}{2}(n_e^3 r_{33}-n_o^3 r_{13})\frac{2\pi L E_z(t)}{\lambda}, \tag{4}$$

with L the effective length of the crystal, n_e and n_o the extraordinary and ordinary indices of refraction, r_{33} and r_{13} the electro-optical coefficients, and $E(t)$ the transient electric field in vacuum directed along the optic axis (z axis), induced by the passage of the relativistic electron beam. This relationship holds when the duration of the electric field is greater than or equal to the time needed by the laser light to traverse the entire length L of the EO crystal.

The electric field induced by a nonrelativistic electron beam is radially symmetric. However, a 45 MeV relativistic beam produces an anisotropically directed radial field orthogonal to the electron beam direction and along the z axis of the EO crystal.[16] The traverse field strength E_z is given by

$$E_z(t)=\frac{1}{4\pi\epsilon_o}\frac{\gamma N_e q T(t)}{\epsilon r^2}, \tag{5}$$

with γ the relativistic Lorentz factor, N_e the number of electrons in the beam, q the electron charge, $T(t)$ the temporal charge distribution, ϵ_o the permittivity of free space, ϵ the dielectric constant of the EO crystal in the z-axis direction, and r the radial distance of the electron beam from the axis of the optical beam. This electron beam field is present for a time[16]

$$\Delta t=\frac{r}{\gamma v}, \tag{6}$$

with v the electron beam velocity. In this experiment Δt is approximately 100 fs which is much shorter than the electron bunch length of ~10 ps. Thus for an uncompressed electron beam, ignoring any nonlinear beam dynamics, the electron bunch length measurement is not distorted. Also, in writing Eq. (6) one approximates the longitudinal size of the electron beam to be negligible compared to the laser beam width. When the longitudinal size of the electron beam is larger than the laser beam width, the electron charge that influences the optical phase of the laser field is only (to first order) the fraction of charge over the laser beam width. The actual strength of the electron beam field is thus lowered due to this geometrical factor.

The effective length L of the crystal is the distance that light travels inside the crystal during the time Δt. When the electron velocity v approaches c, L is given by

$$L=\Delta t\times\frac{c}{n}\simeq\frac{r}{\gamma n}, \tag{7}$$

with n the index of refraction of the crystal at the laser wavelength. Substituting Eqs. (7), (5), and (4) to Eq. (3) gives

$$\left[\frac{I(t)}{I_o}\right]_{\mathrm{EO}}\simeq(n_e^3 r_{33}-n_o^3 r_{13})\frac{N_e q T(t)}{4\lambda n\epsilon_o\epsilon r}. \tag{8}$$

The optical phase is modulated only during the time the electron beam field is present. However, the duration of the EO signal depends on both the electron temporal charge distribution $T(t)$ and the length of the crystal since all the light will be influenced at the same time. Notice that Eq. (8) has no γ dependence, it depends linearly on electron charge $N_e q$, and it has a $1/r$ dependence and not $1/r^2$. Furthermore, the $1/\epsilon$ dependence favors EO crystals with a small dielectric constant.

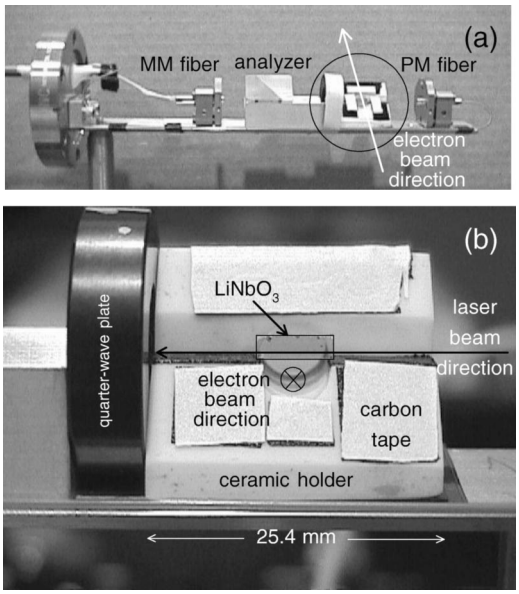

FIG. 1. Experimental setup, (a) showing PM optical fiber input on the right-hand side, followed by the EO crystal and its holder, λ/4 waveplate, analyzer position at 45° crossed to the input polarization, and finally the signal collection multimode fiber, all mounted on an aluminum base plate anchored to a standard vacuum flange. (b) Expanded view of the ceramic holder for the EO crystal. Fluorescent material is placed at various locations of the ceramic holder for on-line guiding of the electron beam to the EO crystal.

II. EXPERIMENTAL ARRANGEMENT

A vacuum compatible EO modulator setup was constructed using discrete optical components mounted on an aluminum bar anchored to a standard 2.75 in. o.d. vacuum flange, see Fig. 1(a). The complete setup was designed to fit into a conventional 1.37 in. i.d. six-way cross, and a 45 MeV electron beam passes through the center of this vacuum beam pipe. The light source was a fiber-coupled, diode-pumped, solid-state, Nd:YAG laser (Coherent Laser Inc.), emitting 250 mW of cw optical power at a wavelength of 1.3 μm. However, in most parts of the experiment, light intensity was attenuated by a factor of 3 using an air-space-gap fiber-optic coupler to avoid the saturation of the photoreceivers and to reduce the possible thermal loading of the EO setup. Active noise suppression electronics were incorporated in this laser to remove the relaxation noise. Beyond 5 MHz rf frequency, the laser noise was ~1 dB above the shot-noise. The polarization purity of the light source had an extinction ratio of $>10^4$ at the output end of the polarization-maintaining (PM) fiber. The light was then coupled to a vacuum sealed PM fiber collimator where the output polarization was rotated to +45° to the azimuthal. The polarization purity dropped to $\sim 10^2$ after one fiber coupling. A 90°-keyed fiber-optic coupler was used to rotate the input polarization to the EO crystal from +45° to −45° as indicated in Fig. 2(b). The collimated 0.4 mm diameter light beam was sent to the bottom

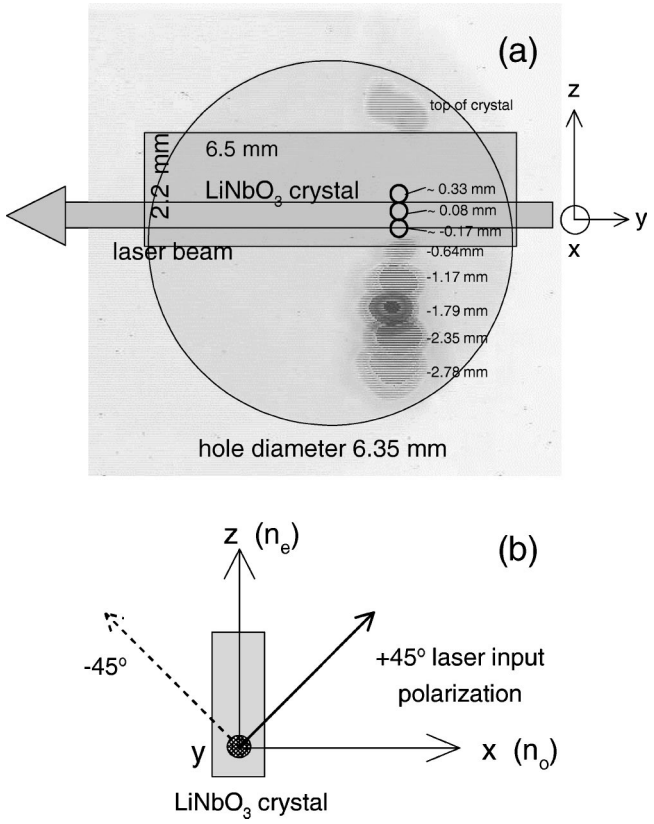

FIG. 2. (a) Schematic drawing of the EO crystal. A 6.35 mm diameter clearance hole on the ceramic holder is also shown. The electron beam propagates along the *x* direction into the paper. Several representative electron beam profiles and their locations with respect to the laser beam position at $z=0$ are overlaid to show the maneuver of the electron beam along the *z* axis passing above, through, and below the EO crystal. Three electron beam positions that were blocked by the EO crystal did not show up clearly on the flag but are illustrated in the figure by their beam positions relative to the laser beam path. Their approximate positions were determined by the pitching current of the dipole magnet. (b) Schematic cross-sectional view of the EO crystal ($1.0\times6.5\times2.2$ mm). The electron beam propagates along the ordinary *x* axis, and the transient electric field is induced along the extraordinary *z* axis of the EO crystal. The laser propagates along the negative *y* axis with a collimated beam diameter of 0.4 mm, its input polarization is oriented either at $+45°$ or $-45°$ to the extraordinary axis.

half of the $LiNbO_3$ EO crystal mounted on a ceramic holder that has a clearance hole of 6.35 mm for the electron beam, see Fig. 1(b). The size of the EO crystal was $6.5\times2.2\times1$ mm; the optical *z* axis (extraordinary axis) was aligned azimuthally and the *x* axis (ordinary axis) was parallel to the propagation direction of the electron beam. Fluorescent material was placed around the 45° facet of the ceramic for guiding the electron beam through the EO crystal. A charge coupled device camera viewed the fluorescence due to the electron beam from directly above the setup. A 45° pop-up flag with the same fluorescent material was located 23 cm downstream of the crystal for precise electron beam location and profile measurements. Each electron beam profile was recorded and overlaid in Fig. 2(a). Three beam profiles where the electron beam traversed the EO crystal did not show up clearly on the flag and their beam position was estimated from the position dependence of the dipole pitching magnet current. A representative beam profile shows the electron beam cleared the top portion of the EO crystal.

To linearize the modulation and balance the residual birefringence of the EO crystal, the $\lambda/4$ wave plate was adjusted so that the EO system was optically biased at the quadrature point. Therefore the resulting electric field-induced optical modulation constantly rode on a large dc light level. However, only the transient component of the optical signal was detected by the optical receiver with the corresponding dc level kept below saturation. An analyzer crossed at $-45°$ to the input polarization was positioned after the crystal. A vacuum sealed multimode (MM) fiber collimator collected the intensity light output after the analyzer. The light throughput of the complete EO setup was ~12%, with typically 5 mW of optical power received by the photoreceiver. The laser source was placed inside the concrete surrounded experimental hall near the EO setup to maintain the high quality of the PM light, but the output light was transmitted by a 40-m long MM fiber to the optical receiver outside the experimental hall for detection and analysis. Light intensity output from the photoreceiver was sent to a digitizing oscilloscope, each signal trace was accumulated in 16–64 signal averages. During the course of the experiment, oscilloscopes with bandwidths of 1, 3, and 7 GHz were used in combination with either a 1 or 12-GHz photoreceiver.

The electron beam source is the 45 MeV electron beam at the Brookhaven National Laboratory Accelerator Test Facility (ATF). A drawing of the ATF layout and its beam lines is shown in Fig. 3. A 5 MeV electron beam from a rf photocathode gun was injected into a linac to boost its energy to 45 MeV. The final beam contained up to a 0.6 nC charge in a focused beam diameter of ~0.5 mm in 10 ps duration at a repetition rate of 1.5 Hz. It was scanned vertically over a range of a few mm from the bottom of the EO crystal to the top of the opening by adjusting the driving current of a dipole pitching magnet. A stable trigger signal synchronized to

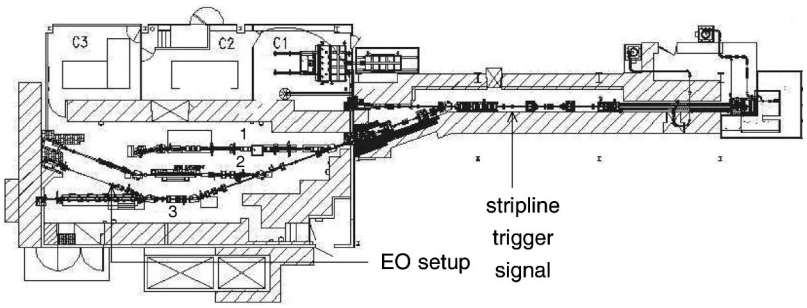

FIG. 3. Accelerator Test Facility (ATF) beam lines. Also indicated are the locations of the EO experiment setup at beam line No. 3 and the trigger signal extracted from a stripline detector at the linac section. Electron beam travels from right to left.

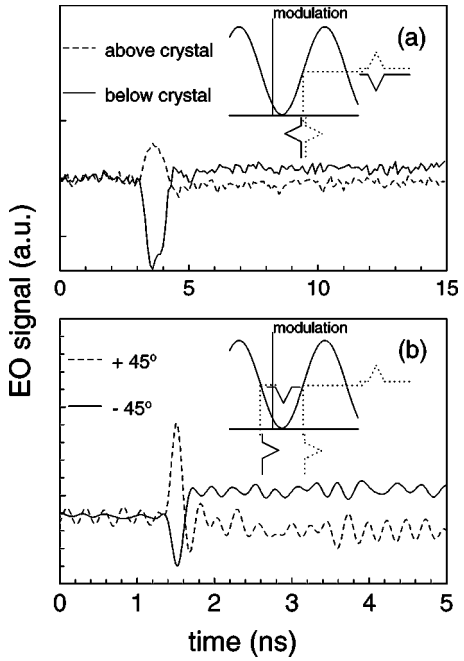

FIG. 4. (a) EO modulated signal when the electron beam passed unobstructed below (solid line) and above (dashed line) the EO crystal so that the induced electron beam field is reversed. (b) EO modulated signal when the input laser polarization was flipped from $+45°$ to $-45°$. Note that the time scale of the two plots are different because a 1- and a 12-GHz photoreceiver was used in (a) and (b), respectively. A pictorial representation of the optical launching condition is illustrated in the inset of each figure.

the electron beam was obtained from a stripline detector upstream, also depicted in Fig. 3.

III. RESULTS

The electron beam induced EO signal was confirmed by a few control experiments. (1) No photons with wavelengths other than the input laser were received by the photoreceiver. Such photons may originate from nonlinear optical processes as well as transition or Cherenkov radiation. (2) The signal vanished in the absence of the electron beam or the laser beam. (3) The signal polarity changed sign when the direction of the induced electrical field was reversed, or (4) when the input laser polarization was rotated by 90°. The results of (3) are shown in Fig. 4(a) where the electron beam was steered above or below the EO crystal inducing opposite electric fields at the path of the laser light causing reversal of the signal polarity. Figure 4(b) also shows a similar polarity flip when the input polarization was changed from $+45°$ to $-45°$ by using a 90°-keyed fiber-optic coupler. We note that the polarization of the input light is maintained when it is coupled either to the fast axis or the slow axis of a PM fiber. The insets of Figs. 4(a) and 4(b), where $I(t)$ in Eq. (1) is plotted, illustrate the simple intuitive explanation of these changes in EO signal polarities. When one operates the EO device on the positive slope of its response function, the polarity of the modulated signal follows the input. However, when the operation moves to the negative slope of its response function, that is equivalent to switching the input polarization from $+45°$ to $-45°$, as shown in Fig. 2(b), the polarity of the modulated signal becomes opposite to the input. It is important to point out that all signal traces with negative (positive) polarity correspond to a light intensity drop (increase). The polarity reversal gives conclusive evidence of the signal being electro-optical in origin.

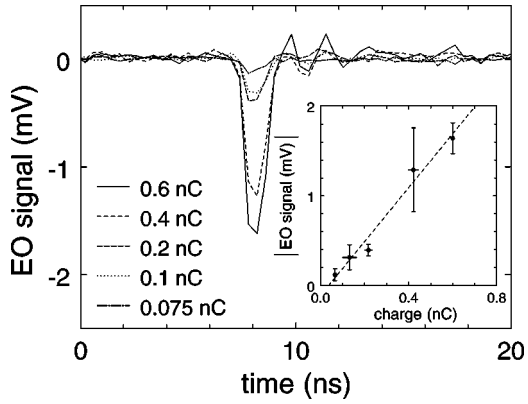

FIG. 5. Increase of the EO modulated signal with electron beam charge. The electron beam position is locked at -1.17 mm away from the laser beam path. The inset shows the dependence of the EO signal with charge, the dashed line is the linear fit to the data.

The EO signal dependence on electron beam charge was also investigated. The electron beam charge was varied by adjusting the UV intensity irradiating the photocathode of the 5 MeV rf electron gun. The actual charge was measured by a Faraday cup before the linac and also by a stripline detector after the linac. Each horizontal error bar displayed in the inset is the difference between these two measuring devices, while each vertical error bar is the standard deviation of six sets of signal traces for each charge. The electron beam position was locked at -1.17 mm away from the laser beam path and it clearly passed below the EO crystal unobstructed. Individual signal traces for five different charges are shown in Fig. 5, and a linear χ-square fit to the signal strength is shown in the inset. A linear dependence of the EO signal with charge was established.

EO signal dependence on electron beam position was also investigated. Figure 6(a) displays five signal traces when the electron beam was steered vertically toward but not traversing the EO crystal. Each electron beam position was indicated in Fig. 2(a) and their amplitudes are plotted against their corresponding distance from the center of the optical beam path in the inset. A χ-square fit of the data favors equally a $1/\sqrt{r}$ or a $1/(r+a)$ dependence, where a is a constant equal to 1.75 mm. On the contrary, the same χ-square fit gives a much lower confidence level on a $1/r^2$ or a linear dependence. Therefore we can conclude that the EO signal behaves very close to but not exactly as predicted in Eq. (8). The discrepancy needs further investigation.

When the electron beam was close to the EO crystal, at beam position -0.64 mm, a distinctive positive signal with a long $\sim$100 ns decay time superimposed on the negative EO modulation was observed. This observation is an indication of the electron beam partially impinging on the EO crystal. A partially blocked electron beam profile observed in Fig. 2(a) also supports this argument. To examine this further, the electron beam was steered to impinge on the EO crystal and traverse the optical beam path completely. Figure 6(b) shows

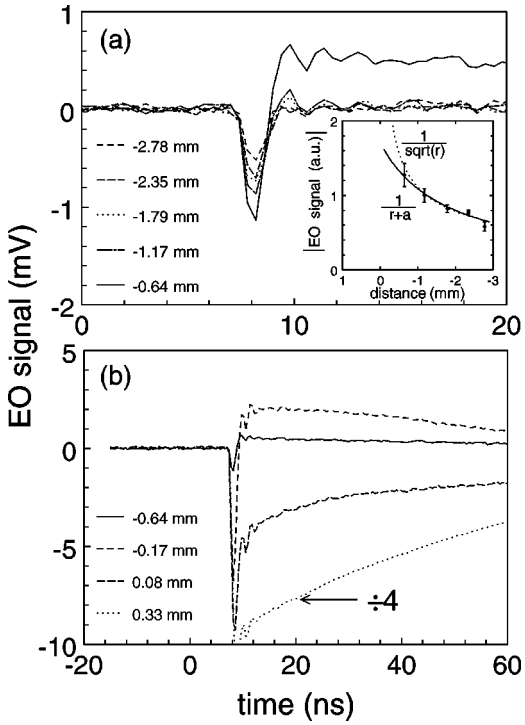

FIG. 6. (a) Increase of the EO modulated signal with the electron beam approaching the EO crystal from the negative z axis. The inset shows the signal plotted against the distance of the electron beam away from the laser beam path. A $1/(r+a)$ and a $1/\sqrt{r}$ dependence is also fitted into the data. (b) Same as (a) but the electron beam was moved to irradiate on the EO crystal and traverse the laser beam path. See Fig. 2 for detailed electron beam positions. Note that the signal trace of -0.64 mm is plotted on both figures for comparison and the data trace of 0.33 mm was divided by a factor of 4 to fit in the current vertical scale.

these signal traces where the time and the amplitude of the signal have both been expanded. As the electron beam approached the optical beam path traversing the EO crystal, the strength of the positive signal increased and then became negative after passing the optical beam path. It is conceivable that the electron beam ionizes the $LiNbO_3$ creating electron–hole pairs. Since the mobility of ions is small compared to the electrons, a transient ion field remains which produces an EO signal opposite to that due to the electron beam field. Its decay time will be dictated by the electron–hole recombination time of the EO crystal.[17] Therefore when the origin of the ion field is moved from below to above the laser beam path, that is from beam position -0.17 to 0.08 mm, the EO signal due to the ionization also changes polarity. Consequently it provides a unique method to locate the exact electron beam position with respect to the laser beam position. However, this ion field fails to diminish when the electron beam continues to move toward the top of the EO crystal as indicated by the data trace obtained at the 0.33 mm beam position in Fig. 6(b). In the present EO design, the signal with negative polarity also corresponds to an intensity drop. Therefore when the electron beam strikes the optical beam path, substantial temporal opacity may be created enhancing the actual strength of the ion field. Nonetheless, the ion field disappears and the electron beam field prevails when the electron beam clears the top of the EO crystal, as shown in Fig. 4(a).

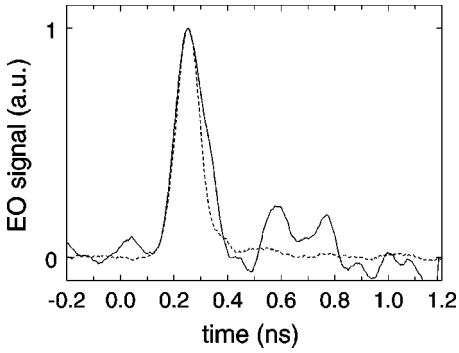

FIG. 7. Solid line: the EO signal detected by a 12-GHz photoreceiver on a 7-GHz digital oscilloscope. Dashed line: instrument response of the measurement system using a ~15 ps IR pulse.

Since the optical modulation is of electro-optical origin which has a response faster than the electron pulse duration, the measured temporal duration is then limited mostly by the bandwidth of the measurement system and the modal dispersion of the 40-m long outgoing MM fiber. The latter effect was independently measured to have negligible temporal broadening on the time scale of interest in this experiment. Figure 7 shows the shortest signal pulse width of 70 ps recorded on a 7-GHz oscilloscope using a 12-GHz optical receiver. The instrument response of the same measurement system is displayed with a dashed line. It is worth pointing out that the instrument response was obtained with a mode-locked IR laser pulse of ~15 ps duration. The rise time and the pulse width of both the instrument response and the EO signal traces are comparable, suggesting that the electron bunch can be inferred to be on the order of ~15 ps.

IV. CONCLUSIONS

The effectiveness of a Pockels cell field sensor has been demonstrated for noninvasive measurement on the bunch length of an ultrashort relativistic electron beam. The signal strength is shown to increase linearly with the charge and decrease inversely with the distance between the laser and the electron beam. Currently the temporal resolution is limited primarily by the detection technique. Although these results are encouraging, at present the EO modulation is at best a few percent of the unmodulated dc light level. Methods to improve the strength of the EO signal and the signal-to-noise ratio are needed to make it more practical. Nevertheless, an EO sensor is clearly an attractive candidate to explore the ultrashort particle bunch duration down to the subpicosecond regime. Measurement of the EO signal using a 2 ps (or a 0.5 ps) resolution limited streak camera is currently underway. Using an upgraded pump–probe EO detection scheme and state-of-the-art ultrafast optical pulse measurement techniques, such as frequency-resolved optical gating or spectral phase interferometry for direct electric-field reconstruction, a relativistic femtosecond electron bunch may be measured. Furthermore, one can in principle construct a two-dimensional ultrafast detector array based on the EO technique to measure the location, spatial, and temporal profile of the charged particle beam. Because the EO modulated signal polarity depends on the induced field direction, the technique

is effective for both positively and negatively charged particles, that is, electrons as well as protons and ions.

ACKNOWLEDGMENTS

We appreciate the assistance of the ATF staff and the AGS vacuum group. This manuscript has been written under Contract No. DE-AC02-98CH10886 with the U.S. Department of Energy.

[1] X. Z. Qui, X. J. Wang, K. Batchelor, and I. Ben-Zvi, Proceedings of the PAC'95, Dallas, TX, 1995, p. 2530.
[2] J. A. Sheridan, D. M. Bloom, and P. M. Solomon, Opt. Lett. **20**, 584 (1995).
[3] D. R. Dykaar, R. F. Kopf, U. D. Keil, E. J. Laskowski, and G. J. Zydzik, Appl. Phys. Lett. **62**, 1733 (1993).
[4] J. C. Santos, M. C. Taplamacioglu, and K. Hidaka, Rev. Sci. Instrum. **70**, 3271 (1999).
[5] A. H. Rose, S. M. Etzel, and K. Rochford, J. Lightwave Technol. **17**, 1042 (1999).
[6] Y. Murooka and T. Nakano, Rev. Sci. Instrum. **63**, 5582 (1992).
[7] W. J. Koshak and R. J. Solakiewicz, Appl. Opt. **38**, 4623 (1999).
[8] Z. Jiang and X. C. Zhang, Opt. Express **5**, 243 (1999).
[9] M. A. Brubaker and C. P. Yakymyshyn, Appl. Opt. **39**, 1164 (2000).
[10] M. Geitz, G. Schmidt, P. Schmüser, and G. V. Walter, NIM **A445**, 343 (2000).
[11] D. Oepts, G. M. H. Knippels, X. Yan, A. M. MacLeod, W. A. Gillespie, and A. F. G. Van der Meer, *Proceedings of the Twentyfirst International FEL Conference*, **II-57** (DESY, Hamburg, Germany, 1999).
[12] Y. K. Semertzidis, V. Castillo, L. Kowalski, D. E. Kraus, R. Larsen, D. M. Lazarus, B. Magurno, T, Srinivasan-Rao, T. Tsang, and V. Usack, Proceedings of the PAC'99, New York, 1999, p.490; Y. K. Semertzidis, V. Castillo, L. Kowalski, D. E. Kraus, R. Larsen, D. M. Lazarus, B. Magurno, D. Nikas, C. Ozben, T. Srinivasan-Rao, and T. Tsang, NIM **A452/3**, 396 (2000).
[13] G. M. H. Knippels, X. Yan, A. M. MacLerd, W. A. Gillespie, M. Yasumoto, D. Oepts, and A. F. G. Van der Meer, Phys. Rev. Lett. **83**, 1578 (1999).
[14] M. J. Fitch, N. Barov, J. P. Carneiro, P. L. Colestock, H. T. Edwards, K. P. Koepke, A. C. Melissinos, and W. H. Harting, FNL Report No. FERMILAB-TM-2096, 1999.
[15] A. Yariv, *Quantum Electronics*, 3rd ed. (Wiley, New York, 1989), p. 315.
[16] J. D. Jackson, *Classical Electrodynamics*, 2nd ed. (Wiley, New York, 1975), p. 555.
[17] E. W. Taylor, J. Opt. Commun. **9**, 64 (1988).